Multiview light-sheet microscope for rapid *in toto* imaging

Uros Krzic[1], Stefan Gunther[1,2], Timothy E Saunders[1,2], Sebastian J Streichan[1] & Lars Hufnagel[1]

We present a multiview selective-plane illumination microscope (MuVi-SPIM), comprising two detection and illumination objective lenses, that allows rapid *in toto* fluorescence imaging of biological specimens with subcellular resolution. The fixed geometrical arrangement of the imaging branches enables multiview data fusion in real time. The high speed of MuVi-SPIM allows faithful tracking of nuclei and cell shape changes, which we demonstrate through *in toto* imaging of the embryonic development of *Drosophila melanogaster*.

Developmental processes are highly dynamic and span many temporal and spatial scales. During development, cells must integrate and respond to a multitude of biochemical and biophysical signals: for example, changes in intracellular signaling networks, cytoskeleton remodeling, cell shape changes, long-range signaling and tissue remodeling[1–3]. A whole-embryo view of morphogenesis with subcellular resolution is essential to unravel the interconnected dynamics at the varying scales of development, from interactions within cells to those acting across the whole embryo. Bridging scales from the submicron to the millimeter range with a temporal resolution of several seconds (combined with a total imaging time of several hours) not only poses tremendous challenges for modern microscopy methods but also requires powerful computational approaches for data handling, processing and image analysis.

The recently rediscovered selective-plane illumination microscopy (SPIM) has emerged as a powerful technique for biological imaging[4–7]. It has proven its potential with specimens ranging from single cells to entire animals[8–10] and has been successfully combined with other modern microscopy methods[11,12]. SPIM generates optically sectioned images of a fluorescent specimen by illuminating only a section of the specimen with a thin light sheet, while the emitted fluorescence is collected by a wide-field microscope that is oriented perpendicular to the light sheet (**Supplementary Fig. 1**). Because SPIM only illuminates the section that is imaged, the biological specimen is exposed to an orders-of-magnitude lower light dose than in a laser-scanning confocal microscope, when hundreds of optical sections are imaged[6]. This makes SPIM especially well placed for imaging entire organisms with sizes of up to a few millimeters.

At macroscopic scales, however, light scattering and absorption in tissues limit image quality, particularly for opaque specimens. To circumvent this issue, rotation of large specimens has previously been used to gain detailed images from multiple angles[13,14]. Specimen rotation has also been shown to improve resolution by reducing the effects of an anisotropic point-spread function (PSF) that is standard to most microscopes (SPIM included)[13,15].

But multidirectional imaging by specimen rotation suffers from three severe drawbacks. First, because the position and orientation of the axis of rotation relative to the specimen are difficult to determine precisely, multiple images obtained by specimen rotation are inherently misaligned[15]. This problem has previously been tackled by unreliable and computationally intensive data-driven image registration algorithms, often necessitating the use of fiducial markers[14]. Second, because of the soft agarose embedding of specimens required for high-quality imaging, rotation is often slower than the biological dynamics, which prevents the synthesis of data from multiple views into a single three-dimensional (3D) intensity distribution. Third, because the quality of marker-free image-based registration decreases rapidly when there is insufficient overlap between neighboring views, a number of viewing directions must be acquired to yield reliable results; this exacerbates the drawbacks in time resolution and increases photobleaching and toxicity. These problems are important reasons why multiview microscopy has yet to become a widely used technique in biology.

To address the above challenges, we have built a new optical setup and an efficient and reliable data processing pipeline that exploits the full potential of multiview SPIM (MuVi-SPIM) microscopy. Our approach reduces the need for specimen rotation and is robust, fast and easy to use. MuVi-SPIM allows, for the first time, the rapid imaging of large fluorescent specimens from multiple directions over biologically relevant timescales, and reconstruction of the images into a single high-quality image in real time. MuVi-SPIM uses two illumination and two detection objective lenses that are focused onto a specimen from four different directions along two perpendicular axes (**Fig. 1a**). A specialized alignment procedure (**Supplementary Protocol**) ensures that both detection objective lenses are focused onto a common focal plane, which is in turn illuminated by the two light sheets. Each light sheet is generated by scanning a Gaussian beam at constant velocity across the specimen[8] through either of the illumination objective lenses (**Fig. 1b**,**c**). Three-dimensional images are accumulated by recording a series of sections while the specimen is moved through the light sheet by a fast piezo stage. The two illumination and detection lenses form four distinct illumination-detection pairs (called imaging branches; see **Fig. 1d**,**e**), each of which

[1]Cell Biology and Biophysics Unit, European Molecular Biology Laboratory, Heidelberg, Germany. [2]Genome Biology Unit, European Molecular Biology Laboratory, Heidelberg, Germany. Correspondence should be addressed to L.H. (hufnagel@embl.de).

RECEIVED 28 NOVEMBER 2011; ACCEPTED 26 APRIL 2012; PUBLISHED ONLINE 3 JUNE 2012; DOI:10.1038/NMETH.2064

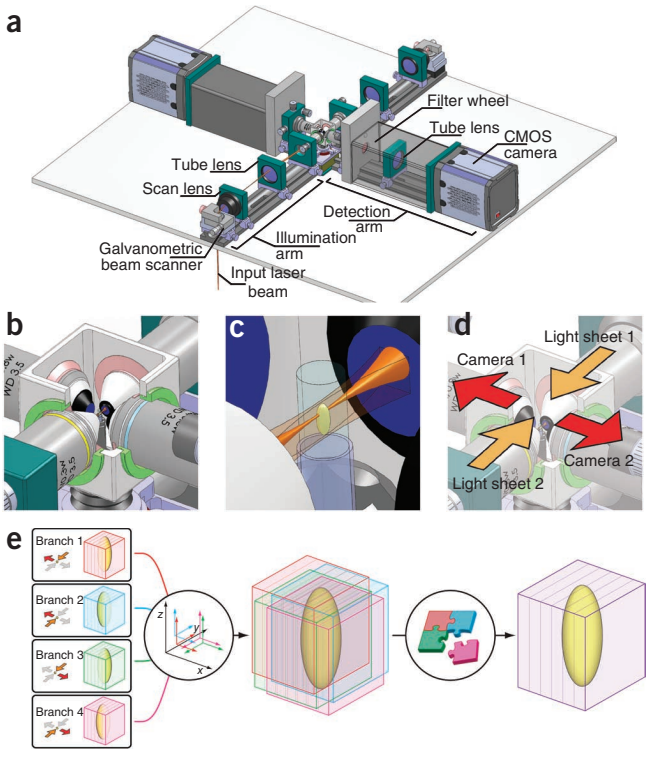

Figure 1 | MuVi-SPIM microscope setup and data processing pipeline. (**a**) MuVi-SPIM setup, consisting of two illumination and two detection arms arranged along two perpendicular axes. (**b**) The water-filled experimental chamber containing the agarose-mounted specimen at the intersection of the illumination and detection axes of the four objectives. (**c**) Specimen mounted in a cylindrical block of agarose and illuminated with a light sheet from one of the illumination arms. (**d**) The two illumination arms (light sheets 1 and 2) and the associated detection arms (camera 1 and 2). Orange arrows indicate the illumination direction and red arrows indicate the direction of the collected emission. (**e**) The four possible illumination-detection combinations (branches) for acquiring four 3D multiview images. Images are first rapidly transformed to a common coordinate system using a predetermined set of transformation parameters and then synthesized into a single high-content image.

produces a 3D image. The four resulting images are sufficient to yield a 3D all-around view of a specimen without rotation. Furthermore, because both detection arms are used simultaneously, MuVi-SPIM has an effective light efficiency twice as high as that of other SPIM implementations. The microscope allows flexibility in defining the temporal sequence of stage motion, light-sheet illumination and detection, enabling users to tailor the operation to the biological dynamics under study. Although in principle MuVi-SPIM allows for illumination of the sample simultaneously from both sides (a mode that would roughly halve the imaging time), it was shown that this tends to reduce the overall image quality because of scattering[16]. Here, we implemented a sequential mode of operation in which each camera records a complete 3D stack from one light sheet before switching to the other light sheet. Real-time electronics ensure the precise timing of all microscopy parts. Because of the mechanical stability of the specimen mounting from below (**Supplementary Fig. 2**), MuVi-SPIM is capable of imaging 3D images with 100 sections per second (see Online Methods and **Supplementary Note 1** for detailed description of the microscope setup and **Supplementary Note 2** for a discussion on imaging speed).

The four views obtained by the imaging branches represent the same fluorophore distribution in the specimen and are therefore linked to each other by a set of geometrical transformations. Translation alone was shown to be insufficient to register multiview SPIM images because of imaging angle–dependent image deformations[15], most notably image scaling (mismatch in magnifications of the two detection arms), image rotation around the detection axis (rotationally misaligned cameras) and skew (piezo translation not parallel to the detection axis). We have therefore used a 3D affine transformation model, which is capable of all first-order image transformations (including the three listed above), to map the four views to a common coordinate system. Parameters of the affine transformation can be efficiently obtained with a diagnostic specimen of fluorescent beads dispersed in agarose. It is important to note that the transformation parameters that link the four views are defined solely by the arrangement of the four optical arms, regardless of what type of specimen (if any) is inserted in the microscope. The parameters determined using the diagnostic specimen therefore remain the same after the specimen is replaced. However, the parameters are subject to the setup stability and will change with time. We have therefore assessed the stability of the MuVi-SPIM setup by imaging dispersed fluorescent beads every 30 min over a 16-h period. During this period, the affine transformation parameters linking the four views drifted less than the equivalent of 0.5 µm relative to each other (**Supplementary Fig. 3**). Hence the parameters defining the relations between the four views, in our case affine transformation coefficients, can be determined before the experiment and will remain valid even for long imaging times.

In order to construct a single image of fluorophore distribution in a specimen (rather than four independent images), all four images are first transformed to a common coordinate system using affine transformation parameters derived from the bead analysis. The four transformed views are then combined to synthesize a single image as a weighted average (**Fig. 1e**, **Supplementary Figs. 4** and **5** and Online Methods); higher weight is given to the parts of each view where the image quality is expected to be best. The geometric transformation and synthesis of four 550-megapixel 3D images (2,560 × 2,160 × 101 pixels) normally requires around 3 s, which is less time than it typically takes to acquire such a multiview image set; MuVi-SPIM can process raw data to high-quality fused images in real time with frame rates of up to 30 two-dimensional sections per second. Notably, unlike in previous multiview SPIM implementations, the quality of the MuVi-SPIM image registration is independent of image content: it performs equally well with specimens that produce images with low intensity or contrast.

We demonstrate the potential of the MuVi-SPIM for *in toto* imaging of morphogenetic processes by recording nuclear positions and cell shapes in the highly dynamic embryonic development of *Drosophila melanogaster*. The *Drosophila* embryo undergoes many rapid and large-scale morphological processes, such as fast nuclear cleavage divisions in the early embryo, ventral furrow formation, germ band extension and dorsal closure. Previous studies were restricted to limited spatial regions of the embryo and only individual morphological processes could be imaged with subcellular resolution. A comprehensive view of the interplay of these processes is thus still lacking. Because MuVi-SPIM yields

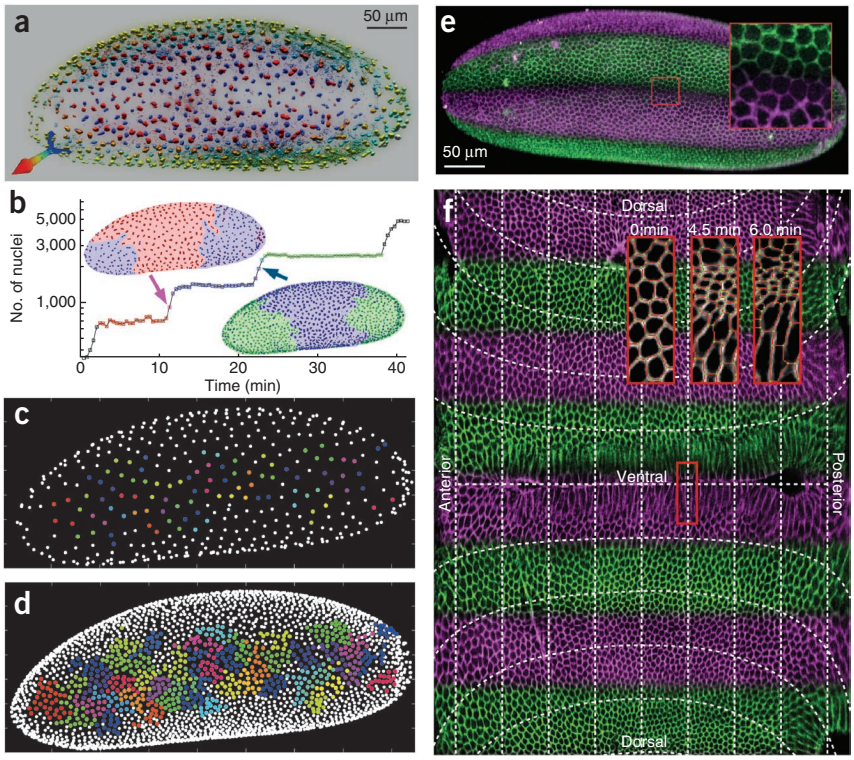

Figure 2 | Rapid and reliable MuVi-SPIM imaging of highly dynamic developmental processes. (**a**) Perspective projection of the fluorescence distribution of an H2Av-mCherry–expressing *Drosophila* embryo in cycle 11. The fused MuVI-SPIM image was median-filtered, had its background subtracted, and then was rendered using Imaris (Bitplane). Color corresponds to the depth of the nuclei in the image; red nuclei are closest and blue nuclei are the farthest (see the colored axes in the bottom left corner). (**b**) Total number of nuclei in every cycle of syncytial blastoderm (note the logarithmic scale). Time is with respect to the beginning of the imaging. Different colors correspond to different cleavage cycles and are used in the embryo outlines to indicate the mitotic front. (**c**,**d**) Graphical representation of nuclei segmentation and tracking in cycle 11 (**c**) and cycle 14 (**d**). Each point corresponds to the center of mass of an individual nucleus, and identical colors corresponds to a common ancestral nucleus in cycle 10. For clarity, only half an embryo is shown. (**e**) 3D image reconstruction of a *Drosophila* embryo expressing the membrane marker Gap43-mCherry in cycle 14. Alternating green and magenta colors correspond to the image contributions from the eight different views. Inset shows a close-up view of the image fusion on the boundary between two different views. (**f**) Modified equirectangular projection of the epidermal layer of an embryo during ventral furrow formation (see **Supplementary Note 4**). The ventral axis corresponds to the central cross-section. Adjacent dashed lines are separated by 50 µm on the 3D embryo surface. Green/magenta shading is the same as in **e**. Insets show segmentation (delineated in red within the boxes) of a subsection during ventral furrow formation. The denoted times correspond to the time after the first segmented image (which is 10 min earlier than the data shown in the main panel of **f**).

quasi-instantaneous 3D fluorophore distributions, it enables us to reconstruct an image of the entire embryo without any mismatches among parts from different imaging branches (**Fig. 2a** and **Supplementary Videos 1–4**).

To test the imaging speed and quality of our embryo image reconstruction, we investigated nuclear division in early *Drosophila* development. In the *Drosophila* blastoderm, mitotic divisions occur up to every 8 min and take less than 1 min to complete[17]. The imaging time for a complete embryo on MuVi-SPIM was around 20 s. Using fused MuVi-SPIM images of embryos expressing a fluorescently tagged histone (H2Av-mCherry) as a nuclear marker (**Fig. 2a**), we could robustly segment and count nuclei from cycles 10–14 (**Fig. 2b**, **Supplementary Video 5** and Online Methods). MuVi-SPIM also enables faithful reconstruction of cell lineages by automatically tracking nuclei, even through several rounds of division (**Fig. 2c**,**d** and **Supplementary Video 6**), and allows for the quantification of nuclei dynamics (**Supplementary Fig. 6**, **Supplementary Video 7**, Online Methods and **Supplementary Note 3**). To demonstrate the potential of MuVi-SPIM for imaging of dense tissues undergoing morphological transformations, we recorded *in toto Drosophila* embryo development starting from early cycle 14 for 15 h (including through gastrulation) using H2Av-mCherry–expressing embryos at high temporal resolution (10-s imaging duration for full embryos, at 30-s intervals) (**Supplementary Video 8**). Several cells from the same region in the ventral ectoderm were selected and tracked through five hours of development and two rounds of division. Following each division, the daughter cells were identified manually and tracked automatically during interphase (see Online Methods for tracking algorithm details). These cells were first arranged along a straight line; then they formed a part of a rosette, later intercalated and finally underwent two rounds of cell divisions. Despite the large-scale morphological motion, these cells (and their progeny) remained closely associated. Example tracks are shown in **Supplementary Figure 7** and **Supplementary Video 9**. This technique provides a powerful approach to understanding the dynamics of tissue development: for example, it can be used to trace cell fate decisions in the *in vivo* context of the tissue.

Although specimen rotation is not required for complete all-around imaging in MuVi-SPIM, it can still lead to improved image quality. The point-spread function of any standard microscope is elongated along the optical axis of the detection objective lens; the microscope's axial resolution is always several times worse than its lateral resolution. In MuVi-SPIM, the resolution along the detection axis is approximately five times worse than perpendicularly to it (with a numerical aperture of 0.8). As demonstrated above, this presents no problem when structures of interest are bigger than the microscope's axial resolution. However, when structures are smaller and/or spaced by distances shorter than the microscope's axial resolution, anisotropic resolution makes analysis of 3D images difficult. For example, on conventional fluorescence microscopes (including SPIM), fluorescent membranes aligned parallel to the long axis of the PSF yield good contrast while perpendicular membranes appear dim, blurred and difficult to resolve (**Supplementary Fig. 8**).

Shape transformations of tissues, tissue migration and remodeling are omnipresent processes during embryonic development[3]. The quantification of cell shape changes is an important step to connect the intracellular dynamics with large-scale changes. But to overcome the limits of the anisotropic resolution, as in other SPIM implementations, the specimen can be rotated in MuVi-SPIM during imaging. After four images of a multiview set are recorded, the specimen is rotated for 90° and another image set is acquired. Hence, the total time taken to complete one imaging cycle is approximately doubled. Despite this, eight-view image sets are collected at least four times faster than in a conventional SPIM.

Figure 2e shows a MuVi-SPIM image of cell membranes in a *Drosophila* embryo during early cycle 14 expressing membrane marker Gap43-mCherry (see Online Methods and **Supplementary Notes 4–6** for fly strain, experimental and image analysis details). Acquiring eight images (two MuVi-SPIM data sets of four images each) of the entire embryo took 43 s, compared to timescales of minutes that were typical in previous attempts to view *Drosophila* embryo in three dimensions using SPIM. Each of the two MuVi-SPIM image sets was fused as described above, and the resulting images were registered using image cross-correlation[18] (Online Methods). As the two intermediate fused images contain much more information than any of the initial eight recordings, this registration step converges reliably and quickly. Moreover, only a single image-driven registration step is required, unlike in conventional SPIM, in which eight rotations and as many registration steps are needed. The resulting image (**Fig. 2e**) demonstrates sufficiently high quality that membrane segmentation was computationally straightforward across the entire embryo surface (**Fig. 2f**) and cell shape changes could be tracked over time (**Supplementary Note 3**, **Supplementary Fig. 9** and **Supplementary Videos 10–12**). Notably, even during rapid morphological changes, such as ventral furrow formation, cell membranes could be fused and segmented at each time point (**Fig. 2f**).

In summary, MuVi-SPIM can record, without rotation, four inherently registered 3D images of a specimen and fuse them into a single high-quality image in real time. It enables rapid *in toto* imaging with subcellular resolution and allows investigation of dynamic biological processes in the context of the entire specimen. It also facilitates efficient and robust image processing. It is important to note that even when rotation is beneficial, such as for imaging cell shapes or improving resolution, MuVi-SPIM still represents a substantial improvement over previous imaging methods for full embryo reconstruction. Here we used single photon illumination to demonstrate the advantages of the MuVi-SPIM configuration. The same arguments should also apply in case of different plane illumination schemes such as non-scanned light sheets[6], Bessel beams or two-photon fluorescence excitation[10,19]. MuVi-SPIM's reliability and speed will make it an important imaging tool to address fundamental questions at the interface between cell and developmental biology.

METHODS

Methods and any associated references are available in the online version of the paper.

Note: Supplementary information is available in the online version of the paper.

ACKNOWLEDGMENTS

We thank the mechanical and electronics workshop of the European Molecular Biology Laboratory (EMBL) for customized hardware; D. Holzer, T. Schneidt and H. Gustafson for help with the flies and G. Heuvelman and M. Wachsmuth for discussions on optics. We thank S. DeRenzis and the Wieschaus laboratory for the Gap43-mCherry flies and E. Lemke for hardware support. We thank J. Ellenberg for his helpful comments on the manuscript and anonymous reviewers for their constructive comments. We acknowledge the advanced light microscopy facility of EMBL for its kind support. We are grateful for financial support from EMBL, the EMBL Interdisciplinary Postdocs Program (EIPOD) and the Center for Modelling and Simulation in the Biosciences (BIOMS).

AUTHOR CONTRIBUTIONS

U.K. and L.H. designed and built the microscope software and hardware. U.K., S.G. and T.E.S. performed the experiments. U.K., S.G., T.E.S. and S.J.S. performed data analysis, quantification and visualization. All authors contributed to the writing of the manuscript.

COMPETING FINANCIAL INTERESTS

The authors declare no competing financial interests.

Published online at http://www.nature.com/doifinder/10.1038/nmeth.2064. Reprints and permissions information is available online at http://www.nature.com/reprints/index.html.

1. Wolpert, L. *et al. Principles of Development* 3rd edn (Oxford University Press, 2006).
2. Lander, A.D. *Cell* **144**, 955–969 (2011).
3. Lecuit, T. *Tissue Remodeling and Epithelial Morphogenesis (Current Topics in Developmental Biology* vol. 89*)* (Academic Press, 2009).
4. Siedentopf, H. & Zsigmondy, R. *Ann. Phys.* **315**, 1–39 (1902).
5. Voie, A.H., Burns, D.H. & Spelman, F.A. *J. Microsc.* **170**, 229–236 (1993).
6. Huisken, J., Swoger, J., Del Bene, F., Wittbrodt, J. & Stelzer, E.H.K. *Science* **305**, 1007–1009 (2004).
7. Dodt, H.-U. *et al. Nat. Methods* **4**, 331–336 (2007).
8. Keller, P.J., Schmidt, A.D., Wittbrodt, J. & Stelzer, E.H.K. *Science* **322**, 1065–1069 (2008).
9. Keller, P.J. *et al. Nat. Methods* **7**, 637–642 (2010).
10. Truong, T.V., Supatto, W., Koos, D.S., Choi, J.M. & Fraser, S.E. *Nat. Methods* **8**, 757–760 (2011).
11. Capoulade, J., Wachsmuth, M., Hufnagel, L. & Knop, M. *Nat. Biotechnol.* **29**, 835–839 (2011).
12. Cella Zanacchi, F. *et al. Nat. Methods* **8**, 1047–1049 (2011).
13. Swoger, J., Verveer, P., Greger, K., Huisken, J. & Stelzer, E.H.K. *Opt. Express* **15**, 8029–8042 (2007).
14. Preibisch, S., Saalfeld, S., Schindelin, J. & Tomancak, P. *Nat. Methods* **7**, 418–419 (2010).
15. Krzic, U. *Multiple-view Microscopy with Light-Sheet Based Fluorescence Microscope.* PhD thesis, Univ. Heidelberg (2009).
16. Huisken, J. & Stainier, D.Y.R. *Opt. Lett.* **32**, 2608–2610 (2007).
17. Foe, V.E. & Alberts, B.M. *J. Cell Sci.* **61**, 31–70 (1983).
18. Goshtasby, A. *2-D and 3-D Image Registration: for Medical, Remote Sensing, and Industrial Applications* (Wiley, 2005).
19. Planchon, T.A. *et al. Nat. Methods* **8**, 417–423 (2011).

ONLINE METHODS

Optical setup. The selective-plane illumination microscope is a fluorescence microscope with which a fluorescent specimen is illuminated from the side with a thin light sheet (**Supplementary Fig. 1**) while the emitted fluorescence is imaged by an objective lens that is perpendicular to the light sheet. Multiview SPIM consists of four optical trains, or 'arms', arranged along two horizontal axes that intersect at a right angle (**Fig. 1a**). Each of the four arms ends with a microscope objective lens that is focused onto a specimen that lies in the intersection of the two microscope axes. Two collinear arms are used to illuminate the specimen and are therefore called illumination arms. Two arms on the axis perpendicular to the former are used to collect the fluorescence generated in the light sheet and record two images with two image sensors. They are referred to as detection arms.

MuVi-SPIM implementation creates a virtual light sheet by scanning a laser beam through the field of view of the detection lens (a method sometimes referred to as digital scanned laser beam light-sheet microscopy, or DSLM), but different methods could also be used in MuVi-SPIM: for example, a static light sheet[6] or a scanning Bessel beam[19]. An illumination arm consists of a galvanometric scanner (VM500+, Cambridge Technology Inc.), scan lens (S4LFT0061/065, Sill optics GmbH and Co. KG), tube lens (TI-E 1×, Nikon Instruments Inc.) and objective lens (CFI Plan Fluor 10×/0.30W, Nikon Instruments Inc.). Each illumination arm is supplied with an illumination laser beam. A set of lasers with different wavelengths (Calypso 491 nm, Samba 532 nm, Jive 561 nm, Mambo 594 nm, all from Cobolt AB) is coupled into a single beam using a set of dichroic beam splitters (LaserMUX, Semrock Inc.) fed through an acousto-optical tunable filter (AOTFnC-400.650, A-A Optoelectronic) that controls the illumination intensity and wavelength, and is coupled into an optical fiber (kineFLEX, Qioptiq Inc.) that transports the light to the microscope. There the beam is collimated (0.7-mm beam diameter) and then diverted into the desired illumination arm using a motorized flip mirror (KSHM 40, Owis GmbH). See **Supplementary Note 5** for light-sheet properties.

Each detection arm resembles a standard epifluorescence microscope and consists of an objective lens (CFI Apo 40×/0.80W or Apo LWD 25×/1.1w, both from Nikon Instruments Inc.), filter wheel (FW-1000, Applied Scientific Instrumentation) with a set of emission filters (LPD01-488RS-25 and BLP01-594R-25, both from Semrock Inc. and HQ525/30, Chroma Technology Corp.), tube lens (NT47-740, Edmund Optics Inc.) and sCMOS camera (Neo, Andor Technology plc.). A 160-mm achromatic converging lens is used as a tube lens, which results in 32× effective magnification. At this magnification, the image of a typical *Drosophila* embryo optimally covers the sCMOS image sensor.

Water-dipping objective lenses used in the four arms require the specimen to be immersed in an aqueous medium. This is made possible by a special experimental chamber featuring four flexible nitrile-rubber membrane seals (**Supplementary Fig. 2a**). The chamber can thus be filled with a liquid while the objective lenses and the chamber remain mechanically uncoupled. This is crucial for the precise positioning of the objective lens and long-term stability of the microscope. Unlike in previous SPIM implementations, the specimen is held in the chamber from below using an original two-stage flexible seal. The latter consists of a Teflon-ring seal, which permits specimen rotation, and a flexible rubber tube, which allows translation of the specimen relative to the chamber. Coarse specimen translation is done using a manual two-axis linear stage (M-401 with two SM-13 Vernier micrometers, Newport Corp.) and motorized vertical stage (M-501, Physik Instrumente GmbH & Co. KG), whereas fine positioning is done by a two-axis piezo stage (P-628.2CL, Physik Instrumente GmbH & Co. KG). The latter is also used to move the specimen through the light sheet to produce the 3D images of the specimen.

To produce focused images, the light sheet must illuminate only a thin section of the sample in the vicinity of the detection objective's focal plane. In MuVi-SPIM, the two light sheets produced by the two illumination arms are aligned with each other using two galvanometric scanners in such a way that they illuminate exactly the same section. The waist of the light sheet (that is, the location along the light sheet where it is the thinnest) is positioned near the intersection of the illumination and detection axes by axially translating the two illumination objectives using two *z* positioners (G061063000, Qioptiq). The two detection objective lenses are then focused onto the illuminated volume using another set of *z* positioners (same as above). One of the detection objective lenses also allows for precise lateral translation along the two directions perpendicular to its optical axis (*xy* stage KT 65, Owis GmbH) in order to make both detection arms image precisely coincident rectangles. Lateral positioning of the illumination objective lenses is not necessary because their magnification is lower than that of the detection illumination lenses. Precise positioning of the light sheets within the field of view of the illumination objective, and their lateral size, are adjusted using the galvanometric scanners.

***Drosophila* strains and genetics.** The H2Av-mCherry construct was derived from H2Av-mRFP[20] (in a pCaSpeR4 vector with endogenous histone regulatory elements, provided by S. Heidmann) by replacing the mRFP sequence with mCherry. Transgenic *Drosophila* lines were obtained by P element–mediated germline transformation of w1118 embryos (Bloomington Stock number 6326). The membrane-labeled Gap43-mCherry fly strain[21] was provided by E. Wieschaus.

Preparation of the diagnostic specimen. The diagnostic specimen was a dispersion of fluorescent beads (Fluoresbrite multifluorescent 0.5-µm beads 24054, Polysciences Inc.) diluted 1:1,000 in 1% agarose solution (agarose N3103-0100, Starlab GmbH) at 80 °C. The dispersion was then sucked into a glass capillary (intraMARK BLAUBRAND, 100 µl, cat. no. 708744, Brand GmbH). After the agarose polymerized, the beads remained immobilized in the aqueous gel, a short segment of which was pushed out of the capillary and imaged in MuVi-SPIM.

***Drosophila* embryo preparation and mounting.** Prior to mounting, embryos were collected using apple juice agar plates and dechorionated for 1–2 min in a fresh 50% bleach solution. Embryos were mounted in an agarose gel inside a glass micropipette (**Supplementary Fig. 2b**). We used 1% low-melting agarose (StarPure Low Melt Agarose, cat. no. N3103-0100, StarLab GmbH), which was dissolved in a phosphate buffered saline (PBS) solution at 80 °C on a magnetic stirrer for 6 h. The semifluid agarose gel was soaked into a disposable micropipette (intraMARK BLAUBRAND, 100 µl, cat. no. 708744, Brand GmbH). The embryo was deposited into molten agarose gel with the embryo's long axis

doi:10.1038/nmeth.2064

parallel to that of the micropipette. After the agarose polymerized, a short segment of the gel cylinder was pushed out of the micropipette (**Supplementary Fig. 2b**). Thus, the embryo was held by the agarose gel alone and separated from the four objective lenses by only water and aqueous gel. The mounting also allowed for unconstrained 360° rotation around the embryo's long axis.

Image fusion. Each of the four possible combinations of an illumination and a detection arm, referred to as imaging branches, generates a 3D image. Four images are normally fused into a single high-quality image (**Supplementary Fig. 4**). Geometric relations between the four images (that is, functions that relate every pixel in one image with corresponding pixels in the remaining three images) are obtained using a diagnostic specimen. A multiview set of four images of the bead dispersion is acquired through the four imaging branches. Images of the bead dispersion are segmented to produce four lists of 3D vectors that correspond to the locations of the beads as imaged through each of the four branches. Affine transformation parameters that optimally mapped each of the vector lists onto a chosen reference list are then obtained as described in **Supplementary Note 6**.

Because the geometric relations between the four views are defined solely by the optical arms (unlike in traditional SPIM implementations, where specimens must be rotated), the transformation parameters stay the same after the diagnostic specimen is replaced with any other fluorescent specimen. Image registration thus becomes a matter of applying the affine transformations to the images. Transformation of one 500-megapixel 3D image on a 16-core PC thus takes approximately 3 s. MuVi-SPIM therefore produces virtually registered multiview image sets in real time. Unlike in previous multiview SPIM implementations, with MuVI-SPIM the quality of the image registration does not depend on the content of the images. The microscope performs identically well with specimens that produce images with low intensity or contrast.

Registered images are then synthesized into a single high-quality image. This image is calculated as a locally weighted average of the four registered views; views that are expected to yield best image quality in a given part of the specimen are given the locally highest weight.

The *Drosophila* embryo weights were calculated as follows: in the first image, the outer shell of the embryo's body was detected. In every view, the total path l of the excitation and emission light through the embryo's body was calculated for every pixel in the 3D image. Weights were then calculated as $e^{-\eta l}$, where η defines the transition length between the views (η = 50 per pixel gives good results and was used to generate **Fig. 2a** and **Supplementary Videos 1**–**4**), and normalized. In effect, the final image is a mosaic of the four input views with sigmoid-like transitions between them (**Supplementary Fig. 4**).

When fluorescent samples are imaged that require rotation (because of the limits of the point-spread function), such as a membrane-marker expressing fly, the image alignment and fusion is more complex. As described in the main text, sample rotation by 90° is required to image the entire embryo in sufficient detail (**Supplementary Fig. 5**). Beads are recorded for each view (0° and 90° rotation), and the four stacks from each viewpoint are aligned and fused as described above (forming two stacks). However, fusing these two stacks into one final 3D image requires image-based registration because the transformations that bind the rotated views are affected by microscopic drift of the specimen relative to the piezo stage and can therefore not be assumed to remain constant[15]. We emphasize that MuVi-SPIM, in this situation, only requires two stacks to be registered using a data-driven algorithm (compared to eight in alternative methods), and that because of the high information content of the two images being registered (each is already a fusion of four images), the image registration is reliable and eight times as fast as conventional multiview SPIM.

The fused image is then calculated as a weighted average of the eight registered views. The *Drosophila* embryo's long axis was detected in the first image, and the volume of the embryo was split into eight cylindrical sectors arranged symmetrically around the embryo axis. The eight sectors of the final image were then assembled, each originating from a different view (**Supplementary Fig. 5a**). Again, transition between two neighboring sectors is softened by weights that resemble a sigmoid function. As only that sector of each view is retained, where the axis of detection arm intersects with the embryo surface under an angle equal to or greater than 45°, tangential resolution in the fused images is everywhere sufficient to resolve neighboring cells (**Supplementary Fig. 5b**). Further details are in **Supplementary Notes 4**–**6**.

Bead analysis and image synthesis were coded in MATLAB (MathWorks Inc.) and the image affine transformation in C++ (Microsoft Visual Studio 2008, Microsoft Corp.) using Insight Toolkit libraries (http://www.itk.org/). Image processing was done on a PC featuring two quad-core 2.4 GHz Intel Xeon CPUs and 48 GB of RAM.

Image analysis of nucleus dynamics in the early *Drosophila* embryo. First we corrected for distortion of the fluorescence distribution due to the point spread function of the microscope using an approximation of the PSF[22] and a parallelized maximum-likelihood deconvolution algorithm[23,24]. The resulting images were then background-corrected using a top-hat filter (**Supplementary Fig. 6a** and **Supplementary Video 1**) and filtered by a Mexican-hat filter, with both filter widths corresponding to the radius of an average nucleus[25].

To obtain the lineage of individual nuclei, the track over time of each nucleus has to be reconstructed. Snapshots of the fluorescence distribution of the nuclei were taken at fixed time steps, which resulted in a discrete spatiotemporal grid of fluorescence distributions. The data analysis was split into two steps: (i) automatic segmentation of the nuclei from the fluorescence distribution, separately for each time point, and (ii) subsequent track reconstruction based on the centroids of the identified objects.

To segment the data, local thresholding yielded a segmentation of candidate objects, which were then kept or discarded based on a volume criterion. Objects with volume greater than the mean volume plus its standard deviation were split into separate objects using a watershed algorithm[26]. **Supplementary Figure 6b** and **Supplementary Videos 5**–**7** demonstrate the segmentation of the nuclei found using this routine.

Once the centroids where obtained, the track reconstruction was reduced to a point-matching problem between consecutive times t and $t + \Delta t$. For two consecutive time points, a centroid pair consists of one member from each of the two time points representing the displacement of a nucleus. Because of the high imaging rate, the displacement of nuclei between subsequent time points

at the chosen temporal resolution did not exceed half the average neighbor distance (**Supplementary Video 5** and **Supplementary Fig. 6d**). Therefore, the tracks could be constructed based on nearest-neighbor point matching. See **Supplementary Note 3** for further details.

Membrane analysis. To image the membrane marker around the entire embryo, we used rotation to ensure that sufficient resolution tangentially to the embryo surface was achieved in all parts of the embryo. For the initial orientation, we imaged as described above for the histone-mCherry expressing embryos (using a 594-nm laser for excitation and an RE594 emission filter), with 2-μm spacing along the *z* axis and 41 ms of exposure time per *z* position. The specimen was then rotated by 90° and imaged again. In effect, for each imaging sequence, eight 3D images were taken. The total time between subsequent images was 51 s (43 s for the four stacks plus the time taken to rotate back to the initial position and reset the light-sheet flip mirror). For each time point, the four image stacks were fused using methods discussed above. In **Supplementary Videos 10** and **12**, we demonstrate a full reconstruction of the embryo during cycle 14.

Images were analyzed using custom-written code in MATLAB (MathWorks Inc.). During early *Drosophila* embryogenesis, the majority of cells lie on the embryo periphery. Therefore, to analyze cell changes, we 'unrolled' the embryo using a modified equirectangular projection (**Supplementary Note 4**).

To analyze the unrolled data set, first background was removed from the data using morphological opening with a 25-pixel-diameter disk size; then a median filter (size 3 × 3) smoothed the data (note that analysis using unsmoothed data was almost identical). To segment the membranes, we took advantage of the MATLAB function *watershed*. Segmentation was generally accurate at all time points (>95% cells correctly segmented), though during ventral and cephalic furrow formation, the segmentation became less reliable and a limited amount of manual correction was required. Manual correction consisted of adjusting only the initial estimate of cell position for the *watershed* function and not the output (that is, given a sufficiently good initial estimate of cell position, the data was of high enough quality to reliably segment). The MATLAB function *bwmorph* was used on the segmented data to detect the cell vertices. In **Supplementary Figure 9a**,**b** we demonstrate segmentation of almost an entire embryo in cycle 14 (pole regions are excluded). We found 4,889 cells, which is consistent with the expected number of cells at this stage.

Tracking of individual nuclei in the ventral ectoderm. A *Drosophila melanogaster* embryo (H2Av-mCherry) was imaged (200 sections spaced by 1 μm) from early cycle 14 for 15 h (at 30-s intervals) and then imaged every 10 min for a further 5 h (imaging time for complete set of four views was 10 s) using MuVi-SPIM with a pair of Nikon Apo LWD 25×/1.1w detection objective lenses. After fusion (as described above), images were filtered with a Mexican-hat filter. Selected nuclei, which would become part of the ventral ectoderm, were tracked through several hours of development with a particle image velocimetry–based tracking algorithm[27].

20. Schuh, M., Lehner, C.F. & Heidmann, S. *Curr. Biol.* **17**, 237–243 (2007).
21. Martin, A.C., Gelbart, M., Fernandez-Gonzalez, R., Kaschube, M. & Wieschaus, E.F. *J. Cell Biol.* **188**, 735–749 (2010).
22. Grill, S. & Stelzer, E.H.K. *J. Opt. Soc. Am. A Opt. Image Sci. Vis.* **16**, 2658–2665 (1999).
23. Quammen, C.W., Feng, D. & Taylor II, R.M. Performance of 3D deconvolution algorithms on multi-core and many-core architectures (Technical Report 09-001) (University of North Carolina at Chapel Hill Department of Computer Science, 2009).
24. Richardson, W.H. *J. Opt. Soc. Am.* **62**, 55–59 (1972).
25. Gonzalez, R.C., Woods, R.E. & Eddins, S.L. *Digital Image Processing Using MATLAB* (Prentice Hall, 2003).
26. Meyer, F. *Signal Process.* **38**, 113–125 (1994).
27. Raffel, M., Willert, C.E. & Kompenhans, J. *Particle Image Velocimetry: A Practical Guide* (Springer, 1998).

doi:10.1038/nmeth.2064